Heliyon 6 (2020) e05197

Contents lists available at ScienceDirect

Heliyon

journal homepage: www.cell.com/heliyon

Research article

Phase states, microstructure and dielectric characteristics of solid solutions $(1 - x)NaNbO_3 - xCa_2Nb_2O_7$ and $(1 - x)NaNbO_3 - xSr_2Nb_2O_7$

J.Y. Zubarev [a], S.-H. Chang [b], C. Lin [b], N.A. Boldyrev [a,*], A.V. Pavlenko [a,c], A.V. Nazarenko [c], A.V. Nagaenko [d], Y.I. Yurasov [a,c], I.A. Verbenko [a], I.A. Parinov [e], L.A. Reznichenko [a]

[a] Research Institute of Physics, Southern Federal University, Rostov-on-Don, Russia
[b] National Kaohsiung University of Science and Technology, Department of Marine Environmental Engineering, Kaohsiung, Taiwan
[c] Southern Scientific Center of the Russian Academy of Sciences, Rostov-on-Don, Russia
[d] Institute for Advanced Technologies and Piezotechnics, Southern Federal University, Rostov-on-Don, Russia
[e] Vorovitch Research Institute of Mechanics and Applied Mathematics, Southern Federal University, Rostov-on-Don, Russia

ARTICLE INFO

Keywords:
Materials science
Materials chemistry
Layered perovskite-like compounds
Ceramics
Calcium pyroniobate
Water intercalation
Phase diagram
Dielectric characteristics

ABSTRACT

Ceramics of binary systems solid solutions $(1 - x)NaNbO_3 - xCa_2Nb_2O_7$ and $(1 - x)NaNbO_3 - xSr_2Nb_2O_7$ with non-isostructural extreme components were prepared by the solid-phase reactions technique with the following sintering using conventional ceramic technology. It was found that ceramics with $x \leq 0.2$ have a perovskite structure. Layered type of structure predominates in the concentration range $0.2 < x \leq 1$. Phase diagrams of both systems at room temperature have been determined in the perovskite area. It was shown that this area contains two concentration regions with the different crystal structures and the morphotropic phase boundary between them. Microstructure and dielectric characteristics of selected solid solutions were investigated. The influence of technological regulations, such as mechanical activation and variation of sintering temperatures, on the formation of the microstructure and dielectric characteristics was studied for the individually selected concentrations ($x = 0.1$ and $x = 0.25$). Dielectric characteristics of ceramics revealed the presence of the Maxwell-Wagner polarization and its corresponding relaxation in the solid solutions $(1 - x)NaNbO_3 - xCa_2Nb_2O_7$ at $x > 0.20$.

1. Introduction

Recently, the perovskite-like layer structured (PLS) ferroelectrics with a formula of $A_nB_nO_{3n+2}$ have received considerable attention because of their wide ranging properties. The properties of $A_nB_nO_{3n+2}$ are related to their unique structure composed of BO_6 octahedra with A cations within the perovskite-like layers, where n is the number of octahedral layers [1, 2]. Ferroelectrics $Ca_2Nb_2O_7$ (CN) and $Sr_2Nb_2O_7$ (SN) are representatives of this class of materials and currently being considered as the basis for many applications. CN is considered as a promising compound for non-linear optics [3], laser technology [4], highly active photocatalyst for water splitting [5, 6], design a multifunctional optical storage device [7, 8]. Both the CN and SN demonstrate mild piezoelectric properties ($d_{33} < 10$ pC/N) with extremely high Curie temperatures (~1800 K and ~1600 K, respectively) [9, 10]. These materials possess very high electrical resistance which decreases with the temperature due to electronic/ionic conduction at elevated temperature [2, 11, 12]. This suggests that CN and SN can found broad application in the aerospace, automotive, and power generating industries [1, 10]. In the past years, appreciable attention has been given to enhance properties of the PLS ferroelectrics by modification [4, 13, 14, 15] and creating new solid solutions [16, 17, 18]. In this work samples of the binary systems solid solutions $(1 - x)NaNbO_3 - xCa_2Nb_2O_7$ (NCN) and $(1 - x)NaNbO_3 - xSr_2Nb_2O_7$ (NSN) were the objects of study. The second component of these systems antiferroelectric $NaNbO_3$ is often used in development of the lead-free industrial piezoceramics. The presence of non-isostructural components (NaNbO3 and pyroniobates) can lead to the appearance of the new phases with unique characteristics and morphotropic phase boundaries (MPB). It is known that MPB in different multiferroic and ferroelectric solid solutions can significantly enhance the performances of the materials [19, 20, 21]. At the same time, production technological regulations (variations in sintering temperature and mechanical activation) also have a strong influence on the phase composition and characteristics of the obtained ceramics. Therefore this work aimed to investigate phase composition, crystal structure, microstructure and dielectric characteristics of NCN and NSN systems and to evaluate the

* Corresponding author.
E-mail address: nboldyrev@sfedu.ru (N.A. Boldyrev).

https://doi.org/10.1016/j.heliyon.2020.e05197
Received 22 October 2019; Received in revised form 15 May 2020; Accepted 6 October 2020

influence of technological regulations on the macroresponces of the obtained solid solutions.

2. Experimental

The binary solid solution systems $(1-x)NaNbO_3 - xCa_2Nb_2O_7$ and $(1-x)NaNbO_3 - xSr_2Nb_2O_7$ were investigated in concentration region $0 \le x \le 1.00$ ($0 \le x \le 0.2$, $\Delta x = 0.025$ and $0.2 < x \le 1.00$, $\Delta x = 0.10$). Ceramic samples were obtained using conventional ceramic technology by double solid-phase synthesis at temperatures $T_1 = (1220 \div 1250)$ K and $T_2 = (1370 \div 1470)$ K depending on composition and holding times $\tau_1 = \tau_2 = 4$ h with following sintering at $T_{Sin} = (1530 \div 1660)$ K during 2.5 h $NaHCO_3$, Nb_2O_5, $CaCO_3$, $SrCO_3$ with the content of the main substance not less than 99.9% were the initial reagents. Samples for sintering were pressed in the form of disks with a diameter of 10 mm and a thickness of 1 mm. After polishing, electrodes were deposited onto flat surfaces of the disks by stepwise firing of the silver paste. Samples with $x = 0.10$ and $x = 0.25$ of both systems were also prepared using mechanical activation to compare their microstructure and macroresponses with other samples (NCN10, NCN25, NSN10, NSN25) (Table 1). Mechanical activation of synthesized powders was carried out using planetary ball millAGO-2. The compositions with the balls of ZrO_2 with a diameter of 8 mm and a total mass of 200 g were loaded into cylinders with an internal diameter of 63 mm. The cylinders with the mixture were placed in a mill, where the powders were mixed up in an alcohol medium for 10 min at a drum rotation speed of 1800 rpm.

X-ray powder diffraction studies were carried out using a diffractometer DRON-3 (Bragg-Brentano focusing, filtered $Co_{K\alpha}$-radiation). In the interval $0.0 \le x \le 0.20$ the parameters of the perovskite monoclinic cell ($a = c \neq b$, $\alpha = \gamma = 90^o \neq \beta$) were calculated using a quadratic form (1) [22]:

$$d_{hkl} = \frac{a \sin\beta}{\sqrt{N}} \left(1 + \frac{k^2}{N} y + \frac{lh}{N} \cos\beta\right) \quad (1)$$

where $N = h^2 + k^2 + l^2$, h, k, l – diffraction indices, $y+1 = b/(a\sin\beta)$. Cell parameters were calculated by the X-ray peaks 200, 020, $\bar{2}02$. The measurement errors of the structural parameters had the following values: $\Delta a = \Delta b = \Delta c = \pm 0.004$ Å, $\Delta\beta = \pm 0.05^o$, $\Delta V = \pm 0.10$ Å^3. To determine the cell multiplicity, experimental X-ray diffraction patterns were compared with theoretical ones computed using original programs.

The experimental density of the ceramics was determined by the method of hydrostatic weighing in octane. The study of the ceramic grain structure was carried out using the KEYENCE VK-9700 color laser scanning 3D microscope.

The study of the ceramics microstructure was carried out using KEYENCE VK-9700 scanning laser microscope. The source of light was a laser with a wavelength of 408 nm. The laser scanning resolution is 2048 × 1536 pixels with a 16-bit photomultiplier. The images were obtained by the method of confocal microscopy. Scanning electron microscope JSM-6390L (JEOL) with a resolution of 1.2 nm at an accelerating voltage of 30 kV was used for more detailed study of the samples microstructure.

Temperature dependences of complex dielectric permittivity $\varepsilon^* = \varepsilon' - i\varepsilon''$ (ε' and ε'' are the real and imaginary parts of ε^*, respectively) were measured at $T = (300 \div 1000)$ K in the frequency range $f = (10^{-3}$ Hz-1 MHz) using impedance analyzers Agilent 4285A, Agilent 4980A and RLC meter E7-20.

3. Results and discussion

It was found (Figure 1) that solid solutions based on $NaNbO_3$ with a perovskite (P) structure are formed in the concentration range $0.00 \le x \le 0.20$ in both systems. The symmetry with increasing x changes from orthorhombic with a quadruple monoclinic subcell O (M_4) to cubic with a superstructure (C_2). Phase transformations occur in sequence O (M_4) → O ($M_4 + M_2$) → O (M_2) → O (M_2) + C_2 → C_2. Two areas of coexistence of phases with different symmetry are established. The first of them is characterized by the coexistence of monoclinic subcells with different multiplicity. The transition from the orthorhombic type of symmetry to cubic is observed in the second concentration range. According to [23], at $x > 0.2$ (P) structure replaced by layered (L(n)) with different values of n. In general, both NCN and NSN systems have almost the same phase diagrams. Minor differences between them include the absence of a pure orthorhombic phase with a doubled monoclinic subsell in the NCN and constant increase of the parameters and volume of the unit cell in the NSN. Presented X-ray diffraction patterns of NCN samples with $x = 0.2$ and 0.25 (Figure 2a) and NSN with $x = 0.2$, 0.25, 0.30 (Figure 2b) shows the transition from the (P) structure to the PLS. It can be seen that NCN25 PLS compound is well structured, while NSN system structure was finally formed only at $x = 0.3$.

Figures 3 and 4 show fragments of microstructures of the NCN and NSN solid solutions, respectively, including basic compounds $NaNbO_3$ (Figure 3a), CN (Figure 3f) and SN (Figure 4f). $NaNbO_3$ has an isometric type of grain structure with crystallites having the shape of a cube. In general, the grain boundaries are thin. Crystallites packing is heterogeneous, grain size varies from 2 μm to ~20 μm. Similar grain structure is observed in the samples of both systems in the (P)-region of the phase diagram (Figures 3a, 3b, 4a, 4b). Further increasing x leads to the change of the type of polycrystallinity. Microstructure becomes anisometric with chaotic oriented grains of acicular and lamellar forms (Figures 3e, 3f, 4e, 4f), which is typical for layered compounds. It correlates with the evolution of the phase composition of the studied systems. The transition from the isometric to the anisometric type of the grain structure occurs in the intermediate concentration range ($0.2 < x < 0.3$) where crystallites of both types coexist (Figures 4c-4e).

Micrographs of the chips of NCN10, NCN25, NSN10 and NSN25 samples obtained at various T_{Sin} are presented on Figures 5 and 6. Both in NCN and NSN increasing T_{Sin} from 1560 K to 1620 K leads to the grain consolidation. It is associated with the activation of diffusion processes and mass transfer at the high temperatures during recrystallization sintering of ceramics. In the NCN10 ceramics from (P)-region of the phase diagram at low $T_{Sin} = 1520$ K microstructure with bulk grains is observed (Figure 5a). But further T_{Sin} increase leads to the formation of the needle-shaped grains (Figures 5b, 5c). It can be caused by presence of the clusters of the layered phase in the (P)-area in NCN solid solution. In solid solutions NSN10 the isotropy of grains is retained over the entire range of T_{Sin} (Figures 6a-6c). In NSN25 located between the perovskite and layered phases, a structure with isotropic grains forms at low T_{Sin} (Figure 6d). A further T_{Sin} rise leads to a significant increase in the average size of grains and a change of their shape to lamellar (Figures 6e, 6f). The difference between the recrystallization processes of NCN10 and NSN10 ceramics cam be explained by the crystal-chemical features of Ca-

Table 1. Densities of the not mechanoactivated and mechanoactivated NCN and NSN solid solutions.

Objects	not mechanoactivated			mechanoactivated		
T_{Sin}, K	1520	1570	1620	1520	1570	1620
density	ρ_{exp}, g/cm^3	ρ_{exp}, g/cm^3	ρ_{exp}, g/cm^3	ρ_{exp}, g/cm^3	ρ_{exp}, g/cm^3	ρ_{exp}, g/cm^3
NCN10	4.46	4.48	4.49	4.2	4.5	4.51
NSN10	4.37	4.44	4.5	3.89	4.47	4.44
NCN25	4.15	4.31	4.44	3.85	4.59	4.61
NSN25	4.22	4.39	4.39	4.31	4.45	4.45

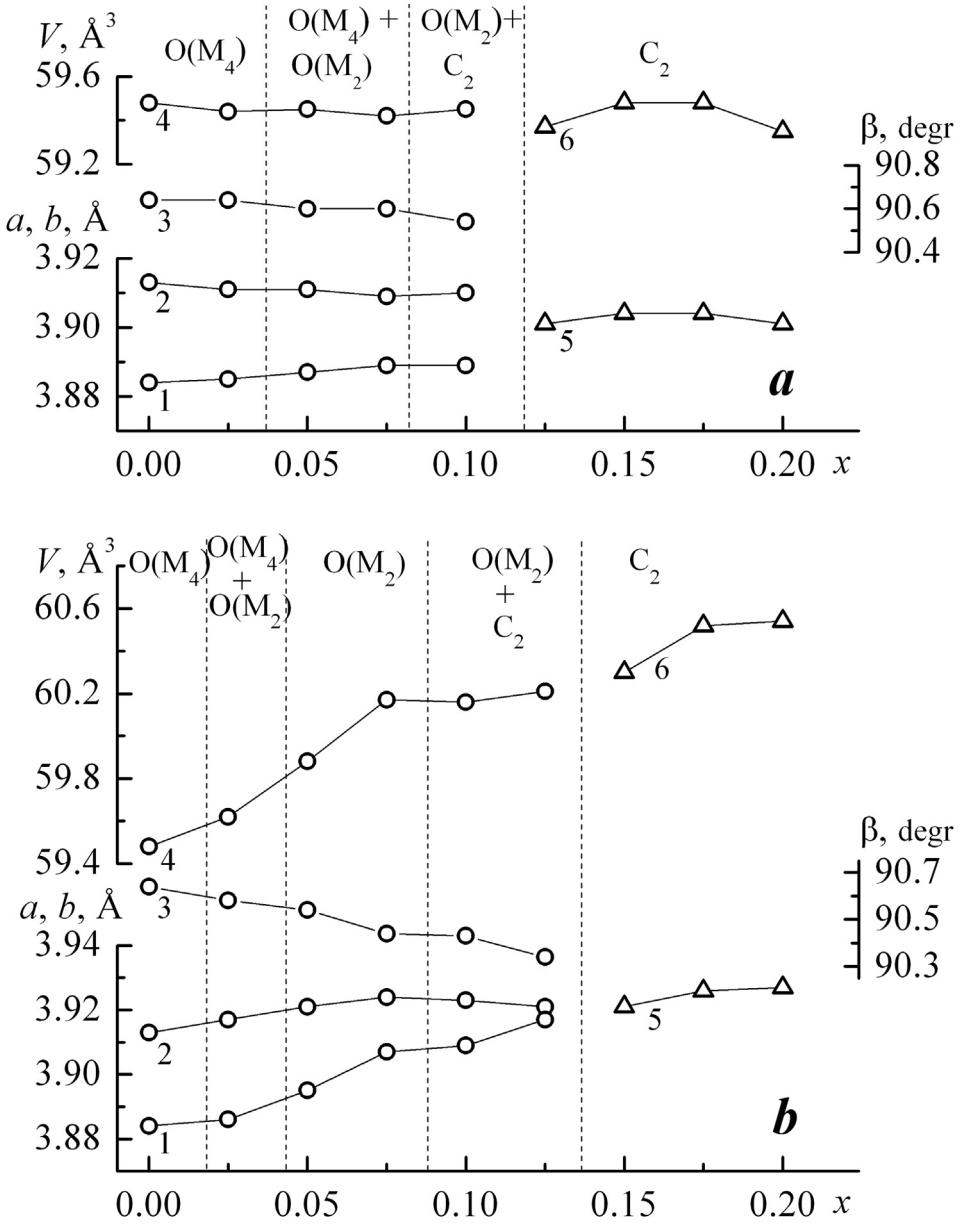

Figure 1. Concentration dependences of the perovskite cell parameters: b_m (1), $a_m = c_m$ (2), β (3), V_m (4), a_c (5), V_c (6) of the NCN (a) and NSN (b) ceramics. Dashed lines indicate phase regions of different symmetries and multiplicities.

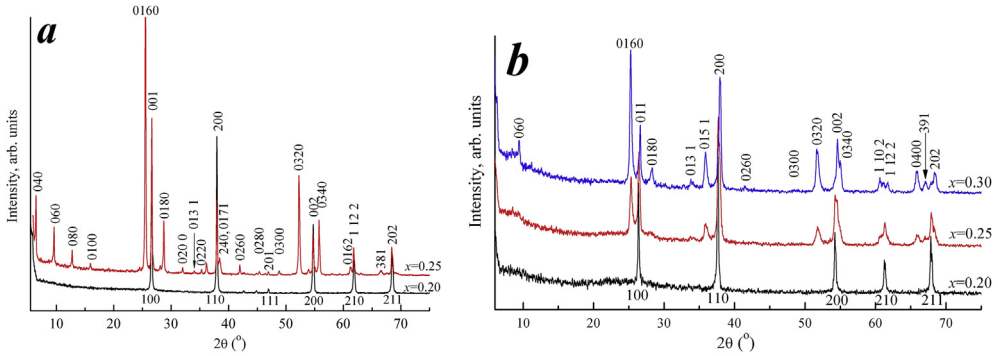

Figure 2. X-ray diffraction patterns of NCN samples with $x = 0.2$ and 0.25 (a) and NSN with $x = 0.2$, 0.25, 0.30 (b), the lower indices refer to the perovskite axes.

containing solid solutions. Unlike strontium cations, the small-sized Ca-cation can be localized in both the A- and B-positions of the perovskite structure that ensures its instability and leads to the formation of clusters of new phases in the NCN10. Mechanical activation has led to the rapid growth of crystallites to gigantic sizes in the NSN25 ceramics. At low T_{Sin}, mechanical activation has led to the appearance of porosity and low

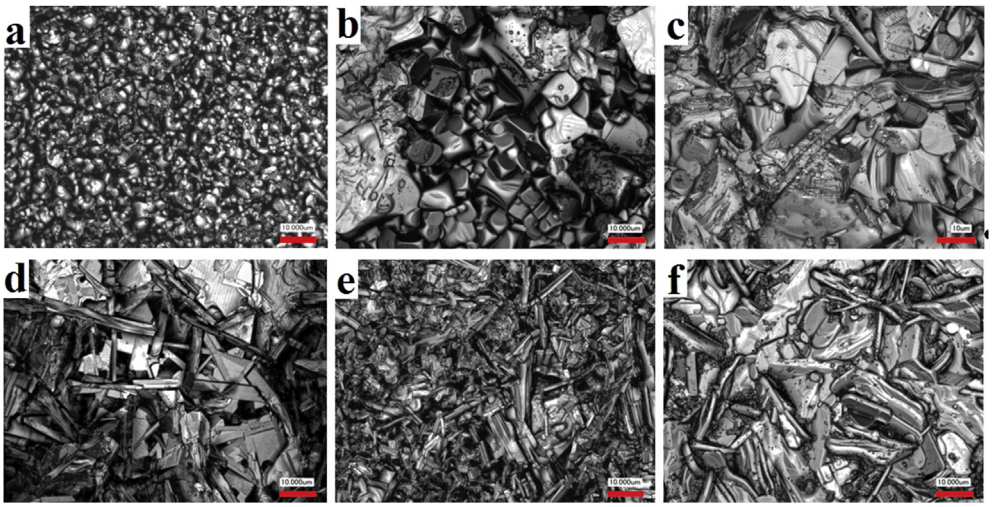

Figure 3. Fragments of the microstructure of the NCN solid solutions (a: $x = 0$, b: $x = 0.175$, c: $x = 0.25$, d: $x = 0.3$, e: $x = 0.55$, f: $x = 1$).

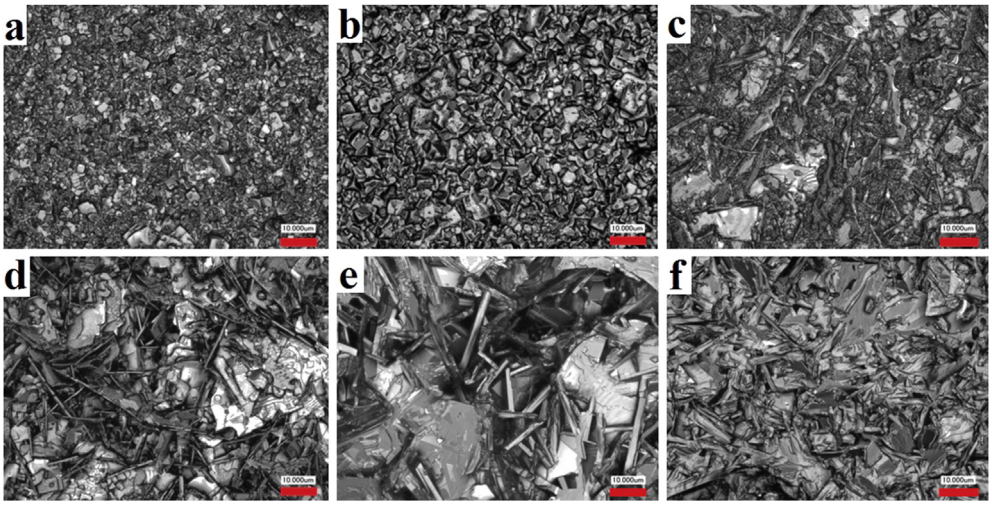

Figure 4. Fragments of the microstructure of the NSN solid solutions (a: $x = 0.05$, b: $x = 0.15$, c: $x = 0.2$, d: $x = 0.25$, e: $x = 0.3$, f: $x = 1$).

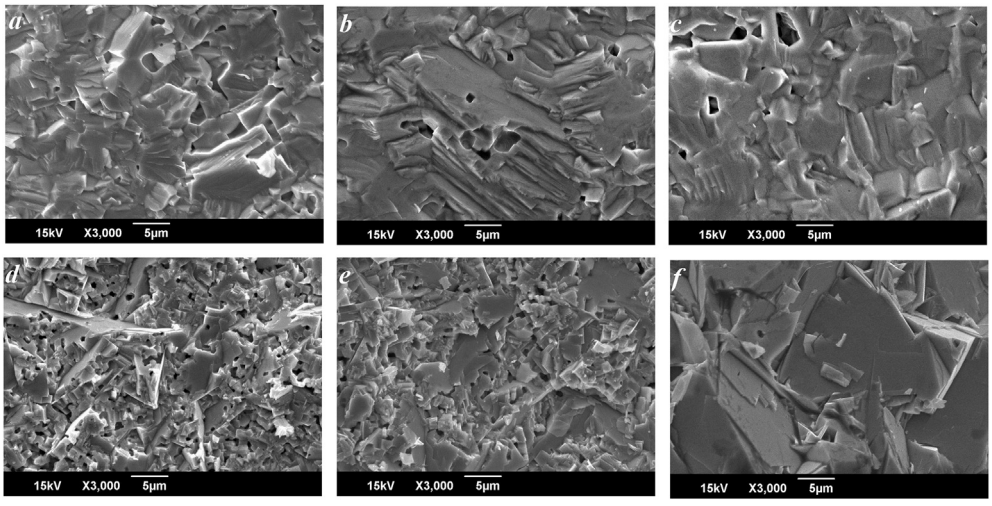

Figure 5. Fragments of the microstructure of the NCN ceramics obtained at various T_{Sin}: $x = 0.10$ (a–c); $x = 0.25$ (d–f); (a, d) $T_{Sin} = 1520$ K; (b, e) $T_{Sin} = 1570$ K; (c, f) $T_{Sin} = 1620$ K.

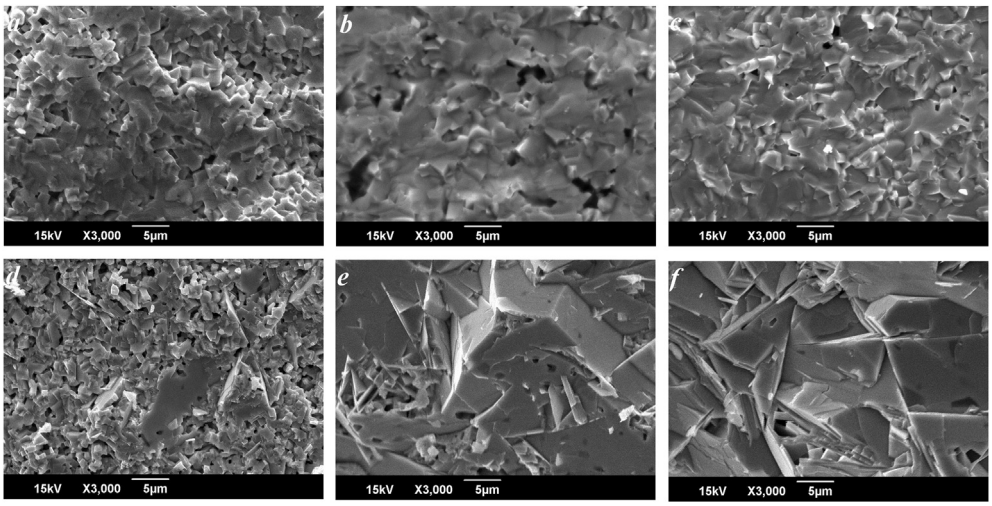

Figure 6. Fragments of the microstructure of the NSN ceramics obtained at various T_{Sin}: $x = 0.10$ (a–c); $x = 0.25$ (d–f); (a, d) $T_{Sin} = 1520$ K; (b, e) $T_{Sin} = 1570$ K; (c, f) $T_{Sin} = 1620$ K.

density of samples (Table 1). However, at high T_{Sin}, the density of mechanically activated ceramics was higher than that of non-mechanically activated analogs. This can be explained by the enhanced formation of primary recrystallization centers during mechanical activation. Moreover, at low T_{Sin} these centers interact with each other weakly, which leads to the formation of structures with weakened grain boundaries and, as a result, to friability and reduced ceramic density.

Temperature dependences of the real part of the relative complex permittivity $\varepsilon'/\varepsilon_0$ and dielectric loss tangent $tg\delta$ at 100 kHz for NCN are presented on Figure 7. Analysis of the dependences $\varepsilon'/\varepsilon_0(T)$ and $tg\delta\ (T)$ in NCN ceramics showed that samples can be divided into two groups. The first group includes compositions from (P)-region with $x \leq 0.2$, which exhibit typical ferroelectrics (antiferroelectrics) $\varepsilon'/\varepsilon_0$ behavior with peaks shifting to the lower temperature region with increasing x. The second group includes compositions with $x > 0.2$, where monotonic increasing $\varepsilon'/\varepsilon_0$ is observed in the studied temperature range. This separation is caused by crystal structure differences between the solid solutions with $x \leq 0.2$ and $x > 0.2$. Similar regularities are observed in NSN solid solutions (Figure 8). However, in addition to the shift of the T_C to the lower temperature region with increasing x, a stronger temperature blurring of the phase transition is observed. It may be associated with an increase in the crystal-chemical disorder in the studied ceramics. NSN solid solutions also demonstrate very low values of the loss tangent, which is three orders of magnitude lower than that in the NCN system. Analysis of the concentration dependences of $\varepsilon'/\varepsilon_0$ at room temperature (Figure 9) and T_C (Figure 9 inset I) revealed the extreme behavior of these values in the range $0.10 < x < 0.20$, where the transition from (P) to (L) structure occurs. It is associated with a decreasing T_C to almost room temperature and lower in this concentration range (Figure 9 inset II).

Figures 10 and 11 make it possible to evaluate how technological procedures affect the dielectric characteristics of ceramics from the perovskite zone. In the NCN10 ceramics (Figure 10a) change in the sintering temperature did not significantly affect the dependences $\varepsilon'/\varepsilon_0(T)$ and $tg\delta(T)$. However, in NSN10 (Figure 10b), increasing T_{Sin} shifted T_C to the high temperature region and reduced phase transition blurring. In both systems, mechanically activated samples have a lower Curie temperature and dielectric loss tangent. It seems difficult to assess the influence of technological regulations on the dielectric spectra of samples from the layered region of the phase diagram (NCN25 and NSN25) due to the character of the changes in $\varepsilon'/\varepsilon_0$ and $tg\delta$ in the research temperature range of 300÷900 K (continuous increasing dielectric constant and the absence of extrema).

In some samples of NCN solid solutions from the concentration range $x > 0.20$, frequency-dependent maxima were observed in the temperature-frequency dependences of the real and imaginary parts of the complex permittivity. These maxima shifted to the high temperatures region and decreased in magnitude as the frequency of the measuring field increased. Figure 12 shows, as an example, the dependences $\varepsilon'/\varepsilon_0(f)$, $\varepsilon''/\varepsilon_0(f)$ and $\varepsilon''/\varepsilon_0\ (\varepsilon/\varepsilon_0')$ at $T = (370 \div 520)$ K in NCN solid solutions with $x = 0.3$.

Studied spectra show the formation of plateaus $\varepsilon'/\varepsilon_0(f)$ at low and high frequencies and maxima of $\varepsilon''/\varepsilon_0(f)$, which are most noticeable in the high frequency region as the temperature elevates. In this case, the shape of dependence $\varepsilon''/\varepsilon_0\ (\varepsilon'/\varepsilon_0)$ (arc of a circle whose center shifted down relative to the ordinate axis) indicates that the observed relaxation belongs to the non Debye type. This type of relaxation suggests the contribution of through conductivity to the dielectric response of the studied samples. Moreover, this contribution can be significant, as previous studies show [24]. A theoretical description of the temperature-frequency dependences of the real and imaginary parts $\varepsilon^*/\varepsilon_0$ in the studied frequency range was carried out in the framework of the linear dielectric model with various relaxation time distribution functions. Approximation of the experimental spectra $\varepsilon'(f)$ and $\varepsilon''(f)$ (Figure 12a and 12b, respectively) was carried out according to formulas (2, 3, 4):

$$\varepsilon' = \varepsilon_\infty + (\varepsilon_s - \varepsilon_\infty)\int_0^\infty \frac{\mathrm{f}(\tau)d\tau}{1+(\omega\tau)^2} \tag{2}$$

$$\varepsilon'' = (\varepsilon_s - \varepsilon_\infty)\int_0^\infty \frac{\omega\tau \mathrm{f}(\tau)d\tau}{1+(\omega\tau)^2} \tag{3}$$

$$\int_0^\infty \mathrm{f}(\tau)d\tau = 1 \tag{4}$$

where ε_s and ε_∞ are the static and high-frequency permittivities, respectively. We used different types of distribution functions of non-interacting relaxators (delta function (Debye distribution), equiprobable distribution, Cole-Cole, Davidson-Cole), however, the best approximation of the experimental results was achieved using the Cole - Cole distribution function of the relaxation times $f(\tau)$ (5):

$$\mathrm{f}(\tau) = \frac{\sin(\alpha\pi)}{2\pi\mathrm{ch}[(1-\alpha)\ln(\tau \mathrm{f}_0)] - \cos(\alpha\pi)} \tag{5}$$

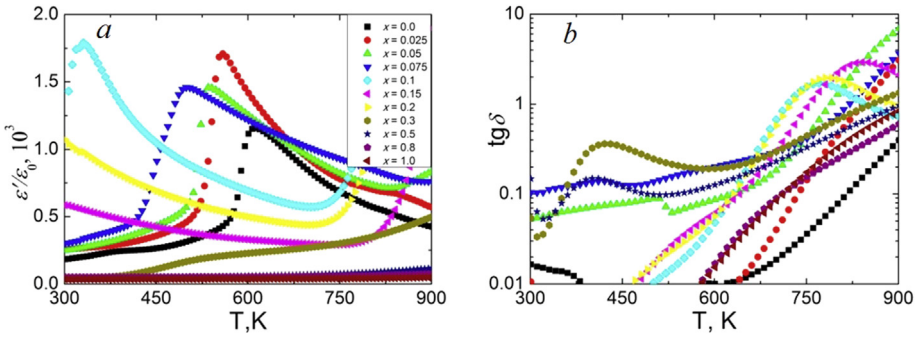

Figure 7. Temperature dependences of $\varepsilon'/\varepsilon_0$ (a) and $tg\delta$ (b) at 100 kHz for NCN solid solutions.

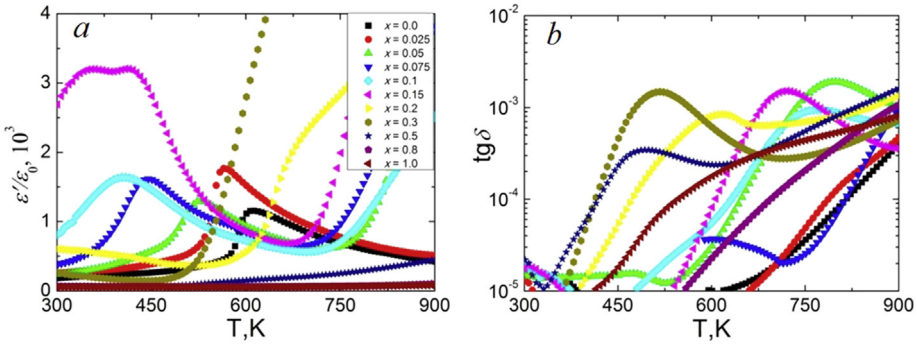

Figure 8. Temperature dependences of $\varepsilon'/\varepsilon_0$ (a) and $tg\delta$ (b) at 100 kHz for NSN solid solutions.

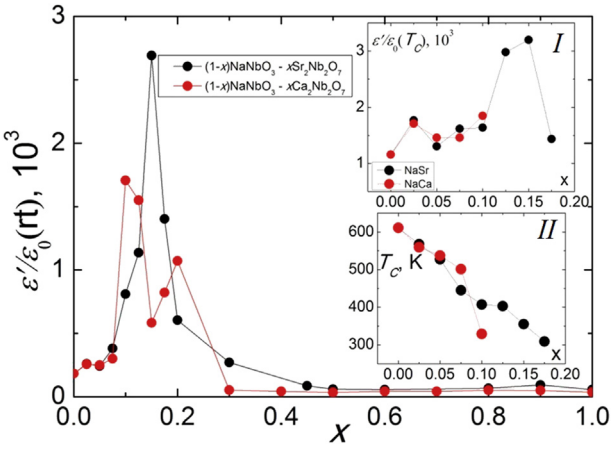

Figure 9. Dependences of $\varepsilon'/\varepsilon_{0(RT)}$ (x), $\varepsilon'/\varepsilon_{0(Tc)}$ (x) (inset I) and $T_C(x)$ (inset II) for NCN and NSN solid solutions.

where α is the exponent parameter which takes a value between 0 and 1, allows describing different spectral shapes. To eliminate the influence of through conductivity the singular term $(\gamma'_{f\to 0}/(2\pi f\varepsilon_0))$, associated with the contribution of the through conductivity, was taken into account at the corresponding frequencies. The approximation results are presented concurrently on Figure 12(c, d, dashed lines).

High values of the parameter α indicate a wide spectrum of the distribution of relaxation times. Similar results were obtained for other $(1-x)NaNbO_3 - xCa_2Nb_2O_7$ solid solutions from the concentration range $x > 0.2$.

Maxwell-Wagner polarization and the corresponding relaxation can be the basis of the physical model describing the observed phenomenon. This type of polarization often called "interlayer", is manifested, in particular, in an electrically inhomogeneous matrix medium consisting of cells of approximately isodiametric ceramic grains (crystallites), which are surrounded by thin layers with high [25] or low [24, 26] conductivity and ε^* different from that of the grains. Observed in this work large variety of grain types, often having different shape and characteristics, leads to the appearance of interlayer polarization and dielectric relaxation in the studied objects.

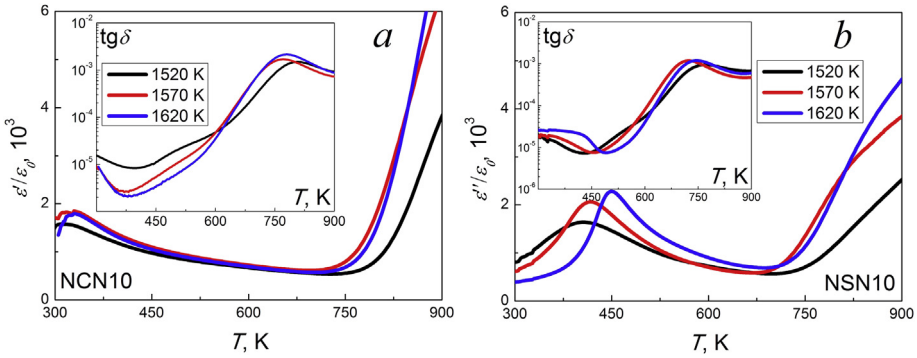

Figure 10. Temperature dependences of $\varepsilon'/\varepsilon_0$ and $tg\delta$ at 100 kHz of the NCN10 (a) and NSN10 (b) ceramics obtained at various T_{Sin}.

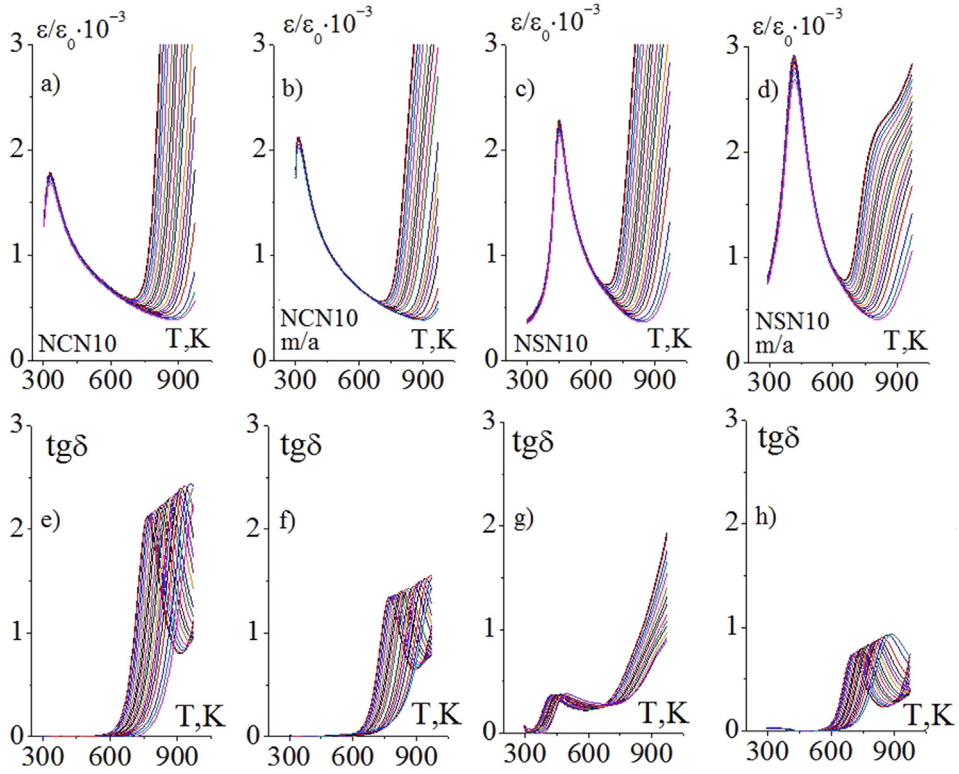

Figure 11. Temperature dependences of $\varepsilon'/\varepsilon_0$ and $tg\delta$ of the non mechanoactivated NCN10 (a, e), mechanoactivated NCN10 (b, f), non mechanoactivated NSN10 (c, g) and mechanoactivated NSN10 (d, h) ceramics obtained at $T_{Sin} = 1620$ K.

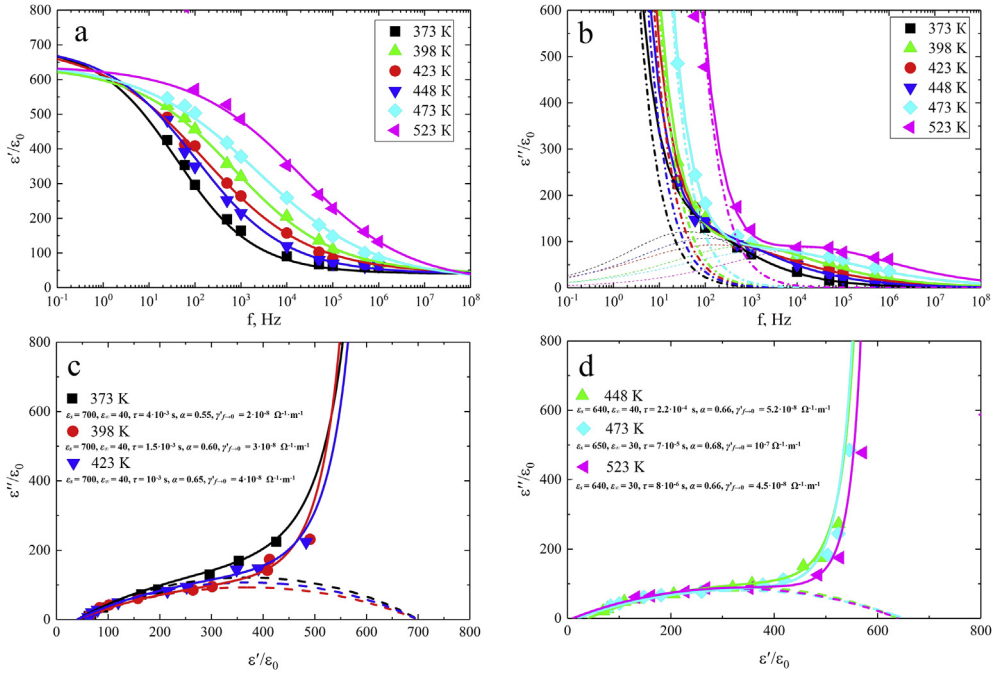

Figure 12. Dependences of $\varepsilon'/\varepsilon_0(f)$ (a), $\varepsilon''/\varepsilon_0(f)$ (b) and $\varepsilon''/\varepsilon_0$ ($\varepsilon'/\varepsilon_0$) (c, d) in the $0.7NaNbO_3 - 0.3Ca_2Nb_2O_7$ solid solutions at 370–520 K (markers). The solid lines correspond to the calculation results for the case taking into account the contribution of the singular term. The dashed lines correspond to the calculation results without taking into account the contribution of the singular term.

4. Conclusions

Solid solutions of the binary systems $(1 - x)NaNbO_3 - xCa_2Nb_2O_7$ and $(1 - x)NaNbO_3 - xSr_2Nb_2O_7$ with non-isostructural extreme components were prepared by solid-phase reaction technique using conventional ceramic technology. Phase diagrams of both systems at room temperature have been determined in the perovskite area. It was shown that this area contains two concentration regions with the different crystal structure and the morphotropic phase boundary between them. The effect of technological regulations on the microstructure and dielectric

responses of the NCN and NSN ceramics was studied. It was found that mechanical activation leads to a slight loosening of the grain structure of ceramics, a shift in the phase transition point to the low-temperature region, and a decrease in dielectric loss. Increasing T_{Sin} leads to enlargement of ceramic grains, and also, in the case of NSN from the perovskite region of the phase diagram, to increase in the Curie temperature and a decreasing phase transition blurring. Using both variations in the sintering temperature and mechanical activation makes it possible to obtain ceramics with a high density, which is a very good result for conventional ceramic technology. It was established that in several samples from layered zones of the phase diagram of both systems, the Maxwell-Wagner polarization and the corresponding relaxation are present. What manifested itself in the presence of frequency-dependent maxima in the dependences $\varepsilon'/\varepsilon_0(T)$ and $\mathrm{tg}\delta(T)$. It was established that the anomalies, which are the consequence of the non-Debye dielectric relaxation and are shifted to the high temperature region with an increase in the frequency of the measuring electric field, are formed in the $(1-x)NaNbO_3 - xCa_2Nb_2O_7$ ceramics from the concentration range $x > 0.2$ on the $\varepsilon'/\varepsilon_0(T)$ and $\varepsilon''/\varepsilon_0(T)$ dependences The most probable cause of the revealed process can be described by Cole - Cole distribution function Maxwell–Wagner relaxation with the wide spectrum of the distribution of relaxation times in the crystallite–interlayer heterogeneous system. The data obtained should be used in the development of new materials based on calcium and strontium pyroniobates.

Declarations

Author contribution statement

Jaroslav Y. Zubarev, Nikita A. Boldyrev, Anatoly V. Pavlenko: Performed the experiments; Wrote the paper.

Shun-Hsyung Chang, Chitsan Lin, Ivan A. Parinov: Analyzed and interpreted the data.

Alexander V. Nazarenko, Alexander V. Nagaenko, Yuri I. Yurasov: Performed the experiments.

Ilya A. Verbenko: Contributed reagents, materials, analysis tools or data.

Larisa A. Reznichenko: Conceived and designed the experiments.

Funding statement

This work was supported by the Ministry of Science and Technology, Taiwan (MOST105-2923-E-022-001-MY3, MOST108-2221-E-992-052-MY2, MOST 108-2221-E-992-026) and the Ministry of Education and Science of the Russian Federation (BAZ 0110/20-3-07IF).

Competing interest statement

The authors declare no conflict of interest.

Additional information

No additional information is available for this paper.

Acknowledgements

We would like to appreciate the Center for Collective Use: "Electromagnetic, Electromechanical and Thermal Properties of Solids" of Research Institute of Physics, Southern Federal University.

References

[1] H. Yan, H. Ning, Y. Kan, P. Wang, M.J. Reece, Piezoelectric ceramics with super-high Curie points, J. Am. Ceram. Soc. 92 (2009) 2270–2275.
[2] H. Ning, H. Yan, M.J. Reece, Piezoelectric strontium niobate and calcium niobate ceramics with super-high Curie points, J. Am. Ceram. Soc. 93 (2010) 1409–1413.
[3] X. Long, X. Han, Growth of nonlinear optical calcium pyroniobate crystal, J. Cryst. Growth 275 (3-4) (2005) 492–495.
[4] C. Wu, Y. Li, H. Gong, J. Gao, Z. Wang, Niobium-oxygen octahedra and oxygen interstitial defect emissions in calcium niobate matrix and its color manipulation via doping Pr^{3+}, AIP Adv. 7 (2017), 025019-1-6.
[5] H.G. Kim, D.W. Hwang, J. Kim, Y.G. Kim, J.S. Lee, Highly donor-doped (110) layered perovskite materials as novel photocatalysts for overall water splitting, Chem. Commun. (1999) 1077–1078.
[6] A. Nakamura, O. Tomita, M. Higashi, S. Hosokawa, T. Tanaka, R. Abe, Solvothermal synthesis of $Ca_2Nb_2O_7$ fine particles and their high activity for photocatalytic water splitting into H_2 and O_2 under UV light irradiation, Chem. Lett. 44 (3) (2015) 1001–1003.
[7] J. Zhang, Y. Long, X. Yan, X. Wang, F. Wang, Creating recoverable mechanoluminescence in piezoelectric calcium niobates through Pr^{3+} doping, Chem. Mater. 28 (11) (2016) 4052–4057.
[8] X. Zhou, Y. Wu, Q. Xie, X. Wang, L. Luo, X. Zhao, et al., Magnetoelectro-optical multifunctional coupling effect in lead-free $BaTiO_3$(Yb/Er)-$CoFe_2O_4$ ceramics, Scripta Mater. 177 (2020) 172–175.
[9] S. Nanamatsu, M. Kimura, Ferroelectric properties of $Ca_2Nb_2O_7$ single crystal, J. Phys. Soc. Jpn. 36 (1974) 1495, 1495.
[10] S. Nanamatsu, M. Kimura, K. Doi, M. Takahashi, Ferroelectric properties of $Sr_2Nb_2O_7$ single crystal, J. Phys. Soc. Japan. 30 (1) (1971) 300–301.
[11] S. Zhang, F. Yu, Piezoelectric materials for high temperature sensors, J. Am. Ceram. Soc. 94 (2011) 3153–3170.
[12] S. Nanamatsu, M. Kimura, T. Kawamura, Crystallographic and dielectric properties of ferroelectric $A_2B_2O_7$ (A=Sr, B=Ta, Nb) crystals and their solid solutions, J. Phys. Soc. Jpn. 38 (1975) 817–824.
[13] P. Sivagnanapalani, B. Sahoo, P. Panda, Calcium niobate based piezo-resistive materials for high temperature sensor application, Ceram. Int. 44 (16) (2018) 20348–20353.
[14] J.-C. Zhang, Y.-J. Liu, X. Yan, H.-D. Zhang, J. Zhang, X. Wang, W.-P. Han, Y.-Z. Long, X.-Y. Sun, Multicolor tuning in room-temperature self-activated $Ca_2Nb_2O_7$ submicroplates by lanthanide doping, ChemPhysChem 18 (3) (2017) 269–273.
[15] C. Pan, J.-C. Zhang, M. Zhang, X. Yan, H.-D. Zhang, Y.-Z. Long, X.-Y. Sun, H.-T. Jiang, Trap-controlled mechanoluminescence in Pr^{3+}-activated $M_2Nb_2O_7$ (M = Sr, Ca) isomorphic perovskites, Opt. Mater. Express 8 (6) (2018) 1425–1434.
[16] T. Chen, R. Liang, Y. Li, Z. Zhou, X. Dong, Structure and electrical properties of perovskite layer $(1-x)Sr_2Nb_2O_7$-$x(Na_{0.5}Bi_{0.5})TiO_3$ high-temperature piezoceramics, J. Am. Ceram. Soc. 100 (2017) 1065–1072.
[17] W. Liu, Ch.H. Mao, G.X. Dong, J. Du Effects of PbO and SrO contents on crystallization and dielectric properties of PbO–SrO–Na2O–Nb_2O_5–SiO_2 glass–ceramics system, Ceram. Int. 35 (3) (2009) 1261–1265.
[18] M. Zhao, X. Ren, W. Pan, Mechanical and thermal properties of simultaneously substituted pyrochlore compounds $(Ca_2Nb_2O_7)_x(Gd_2Zr_2O^7)_{1-x}$, J. Eur. Ceram. Soc. 35 (3) (2015) 1055–1061.
[19] X. Lu, L. Hou, L. Jin, L. Wang, Y. Tian, K. Yu, Q. Hu, L. Zhang, X. Wei, Structure evolution and exceptionally ultra-low hysteresis unipolar electric field-induced strain in $(1-x)NaNbO_3$-$xBaTiO_3$ lead-free ferroelectrics, Ceram. Int. 44 (5) (2018) 5492–5499.
[20] N.A. Boldyrev, A.V. Pavlenko, L.A. Shilkina, A.V. Nazarenko, A.A. Bokov, L.A. Reznichenko, A.G. Rudskaya, E.I. Panchenko, Structure, microstructure, dielectric and piezoelectric properties of (1-x-y)$BiFeO_3$-x$PbFe_{0.5}Nb_{0.5}O_3$-y$PbTiO_3$ ceramics, Ceram. Int. 45 (12) (2019) 14768–14774.
[21] X. Lu, L. Hou, L. Jin, D. Wang, Q. Hu, D.O. Alikin, A.P. Turygin, L. Wang, L. Zhang, X. Wei, Origin of composition-insensitive electrostrictive coefficient and continuous decrease of domain wall density in $(1-x)NaNbO_3$-$xBaTiO_3$ lead-free ferroelectrics, J. Eur. Ceram. Soc. 38 (9) (2018) 3127–3135.
[22] E.G. Fesenko, Perovskite Family and Ferroelectricity, Atomizdat, Moscow, 1972.
[23] J.Y. Zubarev, L.A. Shilkina, L.A. Reznichenko, Phase states and dielectric properties of solid solutions of $(1-x)NaNbO_3$–$xSr_2Nb_2O_7$, $(1-x)NaNbO_3$–$xCa_2Nb_2O_7$ binary systems, Bull. Russ. Acad. Sci. Phys. 80 (11) (2016) 1361–1363.
[24] A.V. Pavlenko, A.V. Turik, L.A. Reznichenko, L.A. Shilkina, G.M. Konstantinov, Dielectric relaxation in the $PbFe_{1/2}Nb_{1/2}O_3$ ceramics, Solid State Phys. 53 (9) (2011) 1872–1875.
[25] O. Raymond, R. Font, N. Suarez, J. Portelles, J.M. Siqueiros, Frequency-temperature response of ferroelectromagnetic $Pb(Fe_{1/2}Nb_{1/2})O_3$ ceramics obtained by different precursors. Part I. Structural and thermo-electrical characterization, J. Appl. Phys. 97 (2005), 084107.
[26] I.P. Raevski, S.A. Prosandeev, A.S. Bogatin, M.A. Malitskaya, L Jastrabik High dielectric permittivity in $AFe_{1/2}B_{1/2}O_3$ nonferroelectric perovskiteceramics (A=Ba, Sr, Ca; B=Nb, Ta, Sb), J. Appl. Phys. 93 (2003) 4130.